

# High-pressure single-crystal X-ray diffraction study of jadeite and kosmochlor

Esther S. Posner · Przemyslaw Dera · Robert T. Downs · John D. Lazarz · Peyton Irmen

Received: 13 January 2014 / Accepted: 29 April 2014 / Published online: 13 May 2014  
© Springer-Verlag Berlin Heidelberg 2014

**Abstract** The crystal structures of natural jadeite, NaAlSi<sub>2</sub>O<sub>6</sub>, and synthetic kosmochlor, NaCrSi<sub>2</sub>O<sub>6</sub>, were studied at room temperature, under hydrostatic conditions, up to pressures of 30.4 (1) and 40.2 (1) GPa, respectively, using single-crystal synchrotron X-ray diffraction. Pressure–volume data have been fit to a third-order Birch–Murnaghan equation of state yielding  $V_0 = 402.5$  (4) Å<sup>3</sup>,  $K_0 = 136$  (3) GPa, and  $K'_0 = 3.3$  (2) for jadeite and  $V_0 = 420.0$  (3) Å<sup>3</sup>,  $K_0 = 123$  (2) GPa and  $K'_0 = 3.61$  (9) for kosmochlor. Both phases exhibit anisotropic compression with unit-strain axial ratios of 1.00:1.95:2.09 for jadeite at 30.4 (1) GPa and 1:00:2.15:2.43 for kosmochlor at 40.2 (1) GPa. Analysis of procrystal electron density distribution shows that the coordination of Na changes from 6 to 8 between 9.28 (Origlieri et al. in *Am Mineral* 88:1025–1032, 2003) and 18.5 (1) GPa

in kosmochlor, which is also marked by a decrease in unit-strain anisotropy. Na in jadeite remains six-coordinated at 21.5 (1) GPa. Structure refinements indicate a change in the compression mechanism of kosmochlor at about 31 GPa in both the kinking of SiO<sub>4</sub> tetrahedral chains and rate of tetrahedral compression. Below 31 GPa, the O3–O3–O3 chain extension angle and Si tetrahedral volume in kosmochlor decrease linearly with pressure, whereas above 31 GPa the kinking ceases and the rate of Si tetrahedral compression increases by greater than a factor of two. No evidence of phase transitions was observed over the studied pressure ranges.

**Keywords** Jadeite · Kosmochlor · Crystal structure · Single-crystal X-ray diffraction · Clinopyroxene · Bulk modulus

E. S. Posner (✉) · R. T. Downs  
Department of Geosciences, University of Arizona, Tucson,  
AZ 85721-0077, USA  
e-mail: Esther.Posner@uni-bayreuth.de

## Present Address:

E. S. Posner  
Bayerisches Geoinstitut, Universität Bayreuth, Bayreuth,  
Germany

P. Dera  
School of Ocean and Earth Science and Technology, Hawaii  
Institute of Geophysics and Planetology, University of Hawaii  
at Manoa, Honolulu, HI 96822, USA

P. Dera · P. Irmen  
Argonne National Laboratory, Center for Advanced Radiation  
Sources, The University of Chicago, Building 434A 9700 South  
Cass Ave, Argonne, IL 60439, USA

J. D. Lazarz  
Department of Earth and Planetary Sciences, Northwestern  
University, Evanston, IL 60208, USA

## Introduction

Pyroxenes are a major component of the Earth's upper mantle, second only to olivine in volumetric distribution. Orthopyroxene transforms to monoclinic symmetry at pressures equivalent to ~225 km depth making clinopyroxene an important phase for storing Si, O, Mg, Fe, Na, Ca, Al, and Cr (Hugh-Jones et al. 1996; Woodland 1998). A recent study by Plonka et al. (2012) reported a high-pressure polymorph of diopside (CaMgSi<sub>2</sub>O<sub>6</sub>) with a 5 % increase in density above 50 GPa and ambient temperature. Due to their large modal abundance, the elastic properties of clinopyroxene end members are necessary to appropriately model the structure of the mantle in accord with seismic observations. The crystal chemistry of pyroxenes at high pressures and temperatures has been summarized by Yang and Prewitt (2000). Structural refinements from

high-pressure in situ X-ray diffraction experiments on jadeite up to 9.17 GPa were reported by McCarthy et al. (2008a, b) and kosmochlor up to 9.28 by Origlieri et al. (2003). Additional studies have investigated the high-pressure behavior along the jadeite–aegirine join up to 8.31 GPa (Nestola et al. 2006), jadeite–hedenbergite join up to 8.31 GPa (Nestola et al. 2008), and the diopside–kosmochlor join up to 6.80 GPa (Boffa Ballaran et al. 2009).

Oceanic and continental crust are both enriched in Na<sub>2</sub>O relative to the upper mantle (Taylor and McLennan 1985). The stability and elasticity of Na-bearing phases at high *P–T* conditions therefore serve as an important tracer of subducted material into the Earth's interior. Albite (NaAlSi<sub>3</sub>O<sub>8</sub>) transforms to jadeite + quartz near the crust–mantle boundary at 2–3 GPa and 1,000 °C (Birch and LeCompte 1960; Newton and Smith 1967; Bell and Roseboom 1969; Holland 1980). Experimental studies at higher *P–T* conditions reveal that jadeite dissociates to a post-spinel calcium ferrite (CF)-type NaAlSiO<sub>4</sub> phase + stishovite at ~23 GPa and 1,000–1,200 °C (Liu 1978; Yagi et al. 1994; Akaogi et al. 2002). First principles computations suggest a significant increase in seismic wave velocities and density associated with jadeite dissociation that may be seismically detectable (Kawai and Tsuchiya 2012). Kosmochlor is a common component of clinopyroxene and, therefore, hosts a significant amount of Cr in the Earth's interior. Extensive kosmochlor–jadeite and kosmochlor–diopside solid solutions have been studied in terrestrial samples (Harlow and Olds 1987; Secco et al. 2002); the latter of which has also been used as a geobarometer (Nimis and Taylor 2000; Nimis 2002). In this study, we report new high-pressure X-ray diffraction data for jadeite up to 30.4 (1) GPa and kosmochlor up to 40.2 (1) GPa at 298 K.

The jadeite and kosmochlor structures are based on an ABAC closest packed arrangement of O atoms and are characterized by chains of corner-linked SiO<sub>4</sub> tetrahedra that run parallel to *c* (Thompson and Downs 2003). Si chains are linked laterally by two distinct M sites; edge-sharing M1-octahedra and larger M2-polyhedra. Na in the M2-site has traditionally been considered to be eight-coordinated based on bond lengths (Clark et al. 1969; Cameron et al. 1973), but electron density and bond-valence sum calculations have also found Na to be in a highly distorted octahedral coordination (Downs 2003). Thompson and Downs (2004) showed that the compressibility of *C2/c* pyroxenes depends primarily on the occupancy of the M1-site. SiO<sub>4</sub> tetrahedra typically undergo very little compression due to strong and short Si–O bonds while the tetrahedral chains themselves are relatively flexible and can rotate to change their chain length along *c*, O3–O3–O3 angle, and Si–Si distance. In this study, we report differences in structural observations and compressibility trends

between jadeite and kosmochlor, which bear Al<sup>3+</sup> and Cr<sup>3+</sup> in M1, respectively.

## Experimental methods

A natural jadeite sample from Clear Creek, San Benito County, California, USA, supplied by Hatt Yoder and numbered R050220 in the RRUFF mineralogical database was used in this study. Jadeite crystals from the same sample were used in the original description of the jadeite structure (Prewitt and Burnham 1966) and high-pressure experimental refinements up to 9.17 GPa (McCarthy et al. 2008a, b). The composition of a jadeite crystal from the same hand specimen was determined by the average of 20 microprobe analyses to be Na<sub>1.002(8)</sub>Al<sub>1.000(10)</sub>[Si<sub>1.979(8)</sub>Al<sub>0.024</sub>]<sub>Σ2.003(8)</sub>O<sub>6</sub>. The kosmochlor crystal used in the diamond anvil cell experiments was numbered R120015 in the RRUFF database and was synthesized by Harlow (1997) from a powdered Na–Cr silicate glass in a muffle furnace at 800 °C for 96 h. Kosmochlor crystals from the same sample were used in high-pressure experimental refinements up to 9.28 GPa (Origlieri et al. 2003). The composition of the synthetic kosmochlor was determined by microprobe to be (Na<sub>0.994</sub>Ca<sub>0.002</sub>)(Cr<sub>0.992</sub>Fe<sub>0.004</sub>Ti<sub>0.002</sub>)Si<sub>2.001</sub>O<sub>6</sub>. Information on these analyses can be found at [www.ruff.info](http://www.ruff.info). Both samples were treated as fully ordered NaAlSi<sub>2</sub>O<sub>6</sub> and NaCrSi<sub>2</sub>O<sub>6</sub>, respectively.

Single crystals of jadeite and kosmochlor were loaded into a symmetric piston-cylinder Princeton-type diamond anvil cell. Diamond anvils with culets of 0.300 mm were mounted on asymmetric backing plates. A rhenium metal gasket pre-indented to 0.040 mm was used for sample containment. The DAC was loaded with a neon pressure medium using the GSECARS/COMPRES gas loading system (Rivers et al. 2008). Pressure was estimated based on the fluorescence spectrum of ruby collected at each pressure point (Mao et al. 1986). Single-crystal X-ray diffraction data were collected at the experimental station 13-ID-D of the GeoSoilEnviroCARS facility at the Advanced Photon Source, Argonne National Laboratory. A monochromatic beam with incident energy of 37 keV, focused with a pair of Kirkpatrick–Baez mirrors to a spot of 0.003 by 0.005 mm was used. Diffraction images were collected using MAR165 charge coupled device (CCD) detector, placed at a sample-to-detector distance of approximately 200 mm. Data collection procedure was the same as described by Dera et al. (2011). Diffraction images were analyzed using the GSE\_ADA/RSV software package (Dera et al. 2013).

**Table 1** Summary of crystal data and refinement results

Jadeite										
$P$ (GPa)	0.0001 <sup>a</sup>	1.9 (1)	5.6 (1)	8.2 (1)	11.8 (1)	12.4 (1)	18.3 (1)	21.5 (1)	30.4 (1)	
$a$ (Å)	9.4242 (2)	9.368 (3)	9.300 (2)	9.243 (3)	9.174 (2)	9.163 (2)	9.082 (3)	9.034 (2)	8.941 (3)	
$b$ (Å)	8.5657 (2)	8.539 (4)	8.447 (3)	8.407 (3)	8.353 (3)	8.340 (4)	8.200 (4)	8.184 (3)	8.025 (4)	
$c$ (Å)	5.2242 (2)	5.1975 (5)	5.157 (1)	5.1220 (5)	5.0850 (9)	5.0739 (5)	5.020 (4)	4.9875 (8)	4.919 (1)	
$\beta$ (°)	107.578 (2)	107.44 (1)	107.14 (2)	106.85 (1)	106.63 (2)	106.52 (9)	106.12 (2)	106.02 (1)	105.59 (2)	
$V$ (Å <sup>3</sup> )	402.03 (2)	396.7 (2)	387.1 (2)	380.9 (2)	373.4 (2)	371.7 (2)	359.2 (2)	354.4 (2)	339.9 (2)	
$\rho_{\text{calc}}$ (g/cm <sup>3</sup> )		3.385	3.468	3.525	3.612		3.739	3.789		
$\mu$ (mm <sup>-1</sup> )		0.602	0.617	0.627	0.642		0.665	0.674		
$F$ (000)		400	400	400	400		400	400		
$\theta$ range for data collection		2.21–17.91	1.56–18.04	2.25–17.93	2.27–17.83		1.60–18.03	1.61–18.11		
No. of reflections collected		508	504	495	526		439	455		
No. of independent reflections		229	213	222	211		189	192		
No. of parameters refined		33	32	33	33		32	32		
Limiting indices		$-11 \leq h \leq 10$ , $-6 \leq k \leq 7$ , $-9 \leq l \leq 9$	$-15 \leq h \leq 15$ , $-10 \leq k \leq 9$ , $-7 \leq l \leq 7$	$-10 \leq h \leq 9$ , $-6 \leq k \leq 7$ , $-9 \leq l \leq 9$	$-12 \leq h \leq 11$ , $-4 \leq k \leq 6$ , $-9 \leq l \leq 9$		$-14 \leq h \leq 14$ , $-9 \leq k \leq 8$ , $-7 \leq l \leq 7$	$-14 \leq h \leq 14$ , $-9 \leq k \leq 8$ , $-7 \leq l \leq 7$		
$R_{\text{int}}$		0.0841	0.1184	0.1020	0.0899		0.1376	0.0905		
Final $R_1$ and $\omega R_2$ (reflections $I > 2\sigma(I)$ )		0.0530, 0.1427	0.0592, 0.1517	0.0485, 0.1262	0.0507, 0.1069		0.0681, 0.1778	0.0613, 0.1405		
Final $R_1$ and $\omega R_2$ (all reflections)		0.0530, 0.1427	0.0635, 0.1518	0.0487, 0.1262	0.0507, 0.1069		0.0681, 0.1778	0.0626, 0.1406		
Goodness of fit		1.388	1.305	1.269	1.074		1.226	1.036		
$\Delta\rho_{\text{max}}, \Delta\rho_{\text{min}}$ (e Å <sup>-3</sup> )		0.467, -0.550	0.640, -0.702	0.543, -0.559	0.582, -0.522		0.640, -0.796	0.598, -1.008		
Kosmochlor										
$P$ (GPa)	0.0001 <sup>b</sup>	2.1 (1)	2.1 (1)	11.3 (1)	18.5 (1)	31.3 (1)	35.3 (1)	40.2 (1)		
$a$ (Å)	9.5720 (3)	9.524 (3)	9.524 (3)	9.328 (4)	9.197 (3)	9.084 (3)	9.067 (3)	9.011 (3)		
$b$ (Å)	8.7094 (2)	8.672 (3)	8.672 (3)	8.466 (4)	8.327 (3)	8.077 (3)	7.971 (4)	7.918 (4)		
$c$ (Å)	5.2678 (2)	5.2411 (5)	5.2411 (5)	5.1310 (9)	5.0572 (6)	4.9544 (6)	4.9309 (7)	4.8955 (8)		
$\beta$ (°)	107.498 (3)	107.36 (1)	107.36 (1)	106.55 (2)	106.23 (2)	105.70 (1)	105.56 (2)	105.10 (2)		
$V$ (Å <sup>3</sup> )	418.84 (3)	413.2 (2)	413.2 (2)	388.4 (3)	371.9 (2)	350.0 (2)	343.3 (2)	337.2 (2)		
$\rho_{\text{calc}}$ (g/cm <sup>3</sup> )		3.652	3.652	4.058	4.058	4.312	4.395	4.474		

Table 1 continued

Kosmochlor								
$\mu$ ( $\text{mm}^{-1}$ )	1.753	1.948	2.07	2.110	2.148			
$F$ (000)	444	444	444	444	444			
$\theta$ range for data collection	1.53–17.54	2.28–18.12	2.34–18.07	2.35–16.97	2.37–17.69			
No. of reflections collected	761	529	502	477	416			
No. of independent reflections	276	212	190	180	157			
No. of parameters refined	35	35	35	35	35			
Limiting indices	$-9 \leq h \leq 10$ , $-9 \leq k \leq 8$ , $-9 \leq l \leq 9$	$-10 \leq h \leq 9$ , $-9 \leq k \leq 7$ , $-9 \leq l \leq 9$	$-10 \leq h \leq 8$ , $-8 \leq k \leq 6$ , $-9 \leq l \leq 9$	$-10 \leq h \leq 9$ , $-8 \leq k \leq 6$ , $-8 \leq l \leq 8$	$-9 \leq h \leq 8$ , $-7 \leq k \leq 6$ , $-8 \leq l \leq 8$			
$R_{\text{int}}$	0.1084	0.1049	0.0982	0.0768	0.1229			
Final $R_1$ and $\omega R_2$ (reflections $I > 2\sigma(I)$ )	0.0494, 0.1225	0.0467, 0.1162	0.0436, 0.1091	0.0494, 0.1070	0.0483, 0.1150			
Final $R_1$ and $\omega R_2$ (all reflections)	0.0499, 0.1227	0.0484, 0.1246	0.0436, 0.1091	0.0581, 0.1095	0.0483, 0.1150			
Goodness of fit	1.115	1.199	1.135	1.162	1.133			
$\Delta\rho_{\text{max}}$ , $\Delta\rho_{\text{min}}$ ( $e \text{ \AA}^{-3}$ )	0.802, -0.793	0.804, -0.672	0.795, -0.836	0.787, -0.827	0.659, -0.661			

Space group =  $C2/c$ <sup>a</sup> Data at ambient pressure are from McCarthy et al. (2008a, b)<sup>b</sup> Origlieri et al. (2003)

**Table 2** Structural parameters of jadeite and kosmochlor as a function of pressure

Sample	Jadeite	Kosmochlor										
M2	1.9 (1)	5.6 (1)	8.2 (1)	12.4 (1)	18.3 (1)	21.5 (1)	2.1 (1)	18.5 (1)	31.3 (1)	35.3 (1)	40.2 (1)	
<i>x</i>	0	0	0	0	0	0	0	0	0	0	0	
<i>y</i>	0.3014 (6)	0.3025 (7)	0.3052 (5)	0.3063 (4)	0.3097 (8)	0.3099 (7)	0.3018 (5)	0.3098 (7)	0.3128 (7)	0.3125 (9)	0.3164 (11)	
<i>z</i>	1/4	1/4	1/4	1/4	1/4	1/4	1/4	1/4	1/4	1/4	1/4	
<i>U<sub>eq</sub></i>	0.014 (1)	0.015 (1)	0.012 (1)	0.015 (1)	0.011 (11)	0.011 (1)	0.014 (2)	0.009 (2)	0.011 (2)	0.008 (2)	0.007 (3)	
M1												
<i>x</i>	0	0	0	0	0	0	0	0	0	0	0	
<i>y</i>	0.0937 (4)	0.0923 (4)	0.0921 (3)	0.0905 (3)	0.0903 (6)	0.0902 (5)	0.0921 (2)	0.0888 (2)	0.0876 (2)	0.0873 (3)	0.0859 (5)	
<i>z</i>	3/4	3/4	3/4	3/4	3/4	3/4	3/4	3/4	3/4	3/4	3/4	
<i>U<sub>eq</sub></i>	0.007 (1)	0.007 (1)	0.007 (1)	0.010 (1)	0.008 (1)	0.006 (1)	0.005 (1)	0.005 (1)	0.005 (1)	0.006 (1)	0.007 (1)	
Si												
<i>x</i>	0.2907 (2)	0.2909 (2)	0.2908 (2)	0.2914 (1)	0.2916 (3)	0.2916 (2)	0.2925 (2)	0.2944 (3)	0.2940 (2)	0.2943 (3)	0.2938 (3)	
<i>y</i>	0.0942 (2)	0.0946 (3)	0.0953 (2)	0.0956 (2)	0.0965 (3)	0.0966 (3)	0.0921 (2)	0.0953 (3)	0.0973 (3)	0.0976 (5)	0.0978 (5)	
<i>z</i>	0.2283 (2)	0.2284 (4)	0.2293 (2)	0.2300 (1)	0.2319 (5)	0.2327 (4)	0.2342 (2)	0.2368 (3)	0.2412 (3)	0.2437 (4)	0.2459 (4)	
<i>U<sub>eq</sub></i>	0.008 (1)	0.008 (1)	0.007 (1)	0.010 (1)	0.009 (1)	0.008 (1)	0.007 (1)	0.006 (1)	0.006 (1)	0.008 (1)	0.005 (2)	
O1												
<i>x</i>	0.1095 (6)	0.1093 (4)	0.1095 (5)	0.1090 (4)	0.1082 (6)	0.1081 (5)	0.1145 (5)	0.1146 (7)	0.1120 (7)	0.1130 (8)	0.1125 (10)	
<i>y</i>	0.0765 (6)	0.0767 (6)	0.0788 (5)	0.0796 (4)	0.0803 (8)	0.0820 (7)	0.0793 (6)	0.0852 (7)	0.0903 (7)	0.0909 (9)	0.0931 (11)	
<i>z</i>	0.1289 (6)	0.1292 (8)	0.1306 (5)	0.1307 (4)	0.1318 (12)	0.1314 (10)	0.1374 (7)	0.1390 (9)	0.1380 (9)	0.1373 (11)	0.1380 (12)	
<i>U<sub>eq</sub></i>	0.007 (1)	0.006 (1)	0.007 (1)	0.008 (1)	0.008 (1)	0.006 (1)	0.008 (1)	0.006 (1)	0.009 (1)	0.006 (1)	0.006 (2)	
O2												
<i>x</i>	0.3598 (6)	0.3609 (5)	0.3587 (5)	0.3600 (3)	0.3594 (7)	0.1396 (5)	0.3595 (5)	0.3588 (8)	0.3578 (1)	0.3556 (8)	0.3535 (10)	
<i>y</i>	0.2648 (7)	0.2669 (7)	0.2677 (5)	0.2694 (6)	0.2731 (10)	0.2717 (8)	0.2596 (6)	0.2674 (9)	0.2710 (8)	0.2734 (11)	0.2760 (14)	
<i>z</i>	0.2952 (7)	0.3021 (11)	0.3020 (5)	0.3077 (3)	0.3150 (12)	0.3189 (10)	0.3065 (6)	0.3276 (9)	0.3417 (9)	0.3447 (12)	0.3468 (13)	
<i>U<sub>eq</sub></i>	0.010 (1)	0.012 (1)	0.009 (1)	0.009 (1)	0.010 (1)	0.008 (1)	0.010 (1)	0.008 (1)	0.010 (1)	0.010 (1)	0.010 (2)	
O3												
<i>x</i>	0.1453 (6)	0.1439 (5)	0.1423 (5)	0.1412 (3)	0.1407 (6)	0.1396 (5)	0.1457 (4)	0.1378 (6)	0.1368 (5)	0.1364 (8)	0.1394 (10)	
<i>y</i>	0.4913 (6)	0.4884 (7)	0.4861 (6)	0.4833 (5)	0.4799 (10)	0.4760 (8)	0.4890 (7)	0.4745 (8)	0.4653 (8)	0.4648 (11)	0.4663 (13)	
<i>z</i>	-0.0052 (6)	-0.0018 (10)	-0.0013 (5)	0.0023 (3)	0.0063 (13)	0.0067 (10)	-0.0075 (6)	0.0043 (9)	0.0057 (8)	0.0049 (11)	0.0068 (12)	
<i>U<sub>eq</sub></i>	0.007 (1)	0.009 (1)	0.007 (1)	0.008 (1)	0.008 (1)	0.007 (1)	0.008 (1)	0.007 (1)	0.008 (1)	0.008 (1)	0.009 (2)	

**Table 3** Atomic displacement parameters ( $\text{\AA}^2$ ) of jadeite and kosmochlor at  $P$ 

	$U_{11}$	$U_{22}$	$U_{33}$	$U_{23}$	$U_{13}$	$U_{12}$
<i>Jadeite</i>						
1.9 (1) GPa						
Na	0.016 (4)	0.014 (5)	0.010 (1)	0	0.002 (2)	0
Al	0.006 (3)	0.011 (4)	0.005 (1)	0	0.002 (1)	0
Si	0.007 (2)	0.011 (2)	0.005 (1)	0 (1)	0.002 (1)	1 (1)
5.6 (1) GPa						
Na	0.015 (3)	0.014 (5)	0.015 (3)	0	0.002 (2)	0
Al	0.007 (2)	0.007 (3)	0.009 (2)	0	0.003 (1)	0
Si	0.004 (1)	0.012 (2)	0.009 (1)	0 (1)	0.002 (1)	−0.001 (1)
8.2 (1) GPa						
Na	0.011 (3)	0.014 (4)	0.008 (1)	0	0.001 (1)	0
Al	0.008 (3)	0.010 (3)	0.005 (1)	0	0.003 (1)	0
Si	0.008 (2)	0.010 (2)	0.004 (1)	1 (1)	0.002 (1)	1 (1)
12.4 (1) GPa						
Na	0.016 (2)	0.019 (4)	0.008 (1)	0	0.002 (1)	0
Al	0.007 (2)	0.019 (3)	0.005 (1)	0	0.002 (1)	0
Si	0.008 (1)	0.015 (2)	0.006 (1)	0 (1)	0.002 (1)	0 (1)
18.3 (1) GPa						
Na	0.014 (3)	0.005 (7)	0.011 (3)	0	0.001 (2)	0
Al	0.008 (2)	0.009 (5)	0.008 (2)	0	0.002 (2)	0
Si	0.005 (2)	0.012 (3)	0.011 (2)	0 (1)	0.003 (1)	0 (1)
21.5 (1) GPa						
Na	0.013 (3)	0.008 (6)	0.011 (2)	0	0.003 (2)	0
Al	0.007 (2)	0.004 (4)	0.007 (2)	0	0.002 (1)	0
Si	0.006 (1)	0.008 (2)	0.010 (1)	−0.001 (1)	0.005 (1)	0 (1)
<i>Kosmochlor</i>						
2.1 (1) GPa						
Na	0.020 (3)	0.008 (4)	0.010 (1)	0	0.001 (1)	0
Cr	0.007 (1)	0.005 (1)	0.004 (1)	0	0.001 (1)	0
Si	0.006 (2)	0.010 (2)	0.006 (1)	−0.001 (1)	0.002 (1)	0 (1)
18.5 (1) GPa						
Na	0.015 (4)	0.004 (5)	0.007 (2)	0	−0.001 (2)	0
Cr	0.003 (2)	0.008 (2)	0.004 (1)	0	0.001 (1)	0
Si	0.004 (2)	0.010 (2)	0.004 (1)	0 (1)	0.001 (1)	0.002 (12)
31.3 (1) GPa						
Na	0.007 (3)	0.016 (5)	0.009 (2)	0	0 (2)	0
Cr	0.007 (1)	0.006 (2)	0.003 (1)	0	0.002 (1)	0
Si	0.006 (2)	0.009 (2)	0.004 (1)	0 (1)	0.001 (1)	0.002 (1)
35.3 (1) GPa						
Na	0.007 (4)	0.008 (6)	0.008 (3)	0	0.001 (2)	0
Cr	0.004 (2)	0.011 (2)	0.002 (1)	0	0.001 (1)	0
Si	0.007 (2)	0.011 (3)	0.004 (1)	−0.002 (1)	0.001 (1)	0.001 (1)
40.2 (1) GPa						
Na	0.013 (6)	0.008 (9)	0.001 (2)	0	0.002 (2)	0
Cr	0.003 (2)	0.015 (3)	0.002 (1)	0	0.001 (1)	0
Si	0.009 (3)	0.001 (4)	0.006 (1)	0.001 (1)	0.001 (1)	0.002 (1)

The initial models for the crystal structure determination were the ambient pressure structures of jadeite (Prewitt and Burnham 1966) and kosmochlor (Clark et al. 1969). The

models were optimized using conventional least squares crystal structure refinement implemented in SHELXL program (Sheldrick 2008). Crystallographic parameters

**Table 4** Selected bond lengths (Å), volumes (Å<sup>3</sup>), distortion parameters, and angles (°) from structure refinements

Sample	Jadeite						Kosmochlor					
<i>P</i> (GPa)	1.9 (1)	5.6 (1)	8.2 (1)	12.4 (1)	18.3 (1)	21.5 (1)	2.1 (1)	18.5 (1)	31.3 (1)	35.3 (1)	40.2 (1)	
<i>R</i> (SiO1)	1.626 (6)	1.621 (5)	1.610 (5)	1.609 (4)	1.606 (6)	1.599 (5)	1.622 (5)	1.590 (7)	1.593 (6)	1.587 (7)	1.581 (9)	
<i>R</i> (SiO2)	1.590 (6)	1.594 (6)	1.580 (5)	1.584 (5)	1.584 (8)	1.571 (6)	1.586 (5)	1.569 (7)	1.548 (6)	1.540 (8)	1.545 (11)	
<i>R</i> (SiO3a)	1.638 (4)	1.630 (5)	1.633 (4)	1.620 (3)	1.603 (7)	1.613 (6)	1.641 (5)	1.631 (6)	1.636 (6)	1.622 (8)	1.591 (9)	
<i>R</i> (SiO3b)	1.630 (4)	1.626 (5)	1.623 (3)	1.618 (3)	1.615 (6)	1.604 (5)	1.634 (4)	1.625 (5)	1.602 (5)	1.599 (6)	1.593 (7)	
<i>R</i> <SiO>	1.621	1.618	1.612	1.608	1.602	1.597	1.621	1.604	1.595	1.587	1.578	
<i>V</i> (SiO <sub>4</sub> )	2.1696	2.1484	2.1335	2.1186	2.0957	2.0770	2.1746	2.108	2.0724	2.0434	2.006	
TAV <sup>a</sup>	21.7965	24.8537	19.5272	19.6644	19.0149	18.6246	15.1407	12.325	12.5376	12.3924	12.0975	
MTQE <sup>b</sup>	1.0051	1.0069	1.0046	1.0047	1.0046	1.0045	1.0036	1.0029	1.0034	1.0033	1.0031	
<i>R</i> (NaO1)	2.350 (7)	2.331 (6)	2.319 (5)	2.298 (4)	2.276 (8)	2.259 (7)	2.376 (6)	2.292 (8)	2.208 (8)	2.187 (9)	2.179 (11)	
<i>R</i> (NaO2)	2.402 (4)	2.365 (6)	2.369 (4)	2.334 (4)	2.305 (7)	2.274 (5)	2.371 (4)	2.261 (6)	2.192 (5)	2.185 (7)	2.195 (8)	
<i>R</i> (NaO3c)	2.706 (5)	2.693 (6)	2.585 (5)	2.522 (4)	2.439 (7)	2.400 (6)	2.739 (5)	2.431 (6)	2.311 (6)	2.295 (8)	2.276 (10)	
<i>R</i> (NaO3d)	2.359 (6)	2.354 (7)	2.337 (5)	2.333 (3)	2.314 (9)	2.326 (7)	2.404 (6)	2.361 (7)	2.348 (8)	2.329 (9)	2.301 (11)	
Diff <sup>c</sup>	0.356	0.308	0.266	0.224	0.163	0.141	0.368	0.170	0.156	0.144	0.122	
<i>R</i> <NaO>	2.454	2.428	2.402	2.372	2.333	2.314	2.473	2.336	2.265	2.249	2.238	
<i>V</i> (NaO <sub>8</sub> )	24.2091	23.5761	22.8774	22.0160	21.0849	20.6186	24.9231	21.3278	19.6649	19.3497	19.135	
<i>R</i> (M1O1a)	1.934 (4)	1.924 (4)	1.922 (3)	1.908 (2)	1.897 (6)	1.885 (5)	2.001 (3)	1.955 (5)	1.916 (5)	1.910 (5)	1.907 (6)	
<i>R</i> (M1O1b)	1.987 (5)	1.957 (5)	1.954 (4)	1.929 (4)	1.898 (7)	1.900 (6)	2.031 (5)	1.964 (6)	1.928 (6)	1.919 (7)	1.904 (9)	
<i>R</i> (M1O2)	1.851 (6)	1.835 (6)	1.835 (5)	1.819 (4)	1.795 (7)	1.801 (5)	1.942 (5)	1.886 (7)	1.870 (6)	1.869 (7)	1.858 (9)	
<i>R</i> <M1O>	1.924	1.905	1.904	1.885	1.864	1.862	1.991	1.935	1.905	1.899	1.893	
<i>V</i> (M1O <sub>6</sub> )	9.2999	9.0418	9.0229	8.7684	8.4449	8.4352	10.4042	9.5425	9.0466	8.9474	8.8388	
OAV <sup>a</sup>	47.2915	45.2320	44.3271	42.0083	47.4905	45.1854	27.7456	28.8548	42.0251	49.2869	54.4445	
MOQE <sup>b</sup>	1.0148	1.0142	1.0138	1.0131	1.0148	1.0139	1.0084	1.0087	1.0122	1.0141	1.0155	
Si–O3–Si	138.5 (3)	137.4 (3)	136.2 (3)	135.45 (17)	134.4 (4)	133.1 (3)	139.1 (3)	133.0 (4)	129.9 (3)	129.6 (5)	130.9 (6)	
O3–O3–O3	173.5 (1)	171.3 (3)	169.6 (1)	167.5 (1)	165.0 (3)	162.1 (4)	171.7 (3)	160.9 (3)	154.5 (4)	154.4 (4)	155.4 (5)	

<sup>a</sup> TAV/OAV tetrahedral/octahedral angle variances

<sup>b</sup> MTQE/MOQE mean tetrahedral/octahedral quadratic elongation

<sup>c</sup> Diff length differences between the longest and shorted reported Na–O bonds

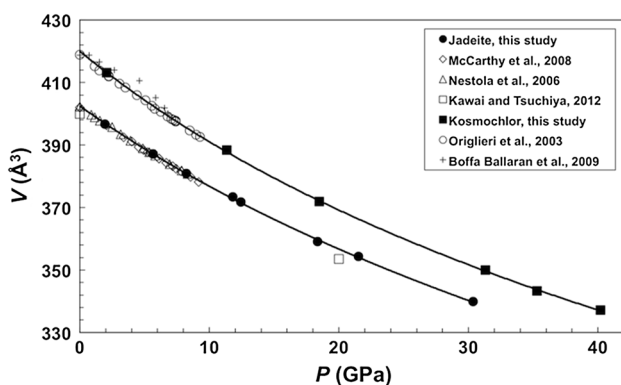


**Fig. 1** Unit-cell volume as a function of pressure for jadeite and kosmochlor. Data are fit with a third-order Birch–Murnaghan equation. Kosmochlor has a larger cell than jadeite because Cr<sup>3+</sup> in the octahedral M1 site has a larger ionic radius than Al<sup>3+</sup>

for structure refinements are summarized in Table 1, final atomic coordinates and isotropic displacement parameters in Table 2, anisotropic displacement parameters in Table 3, and selected bond distances, angles, and distortion parameters in Table 4.

## Results and discussion

Pressure–volume equations of state for jadeite and kosmochlor were obtained by fitting a third-order Birch–Murnaghan equation of state to data from Table 1, resulting in  $V_0 = 402.5 (4) \text{ \AA}^3$ ,  $K_0 = 136 (3) \text{ GPa}$ , and  $K'_0 = 3.3 (2)$  for jadeite and  $V_0 = 420.0 (3) \text{ \AA}^3$ ,  $K_0 = 123 (2) \text{ GPa}$ , and  $K'_0 = 3.61 (9)$  for kosmochlor. Our jadeite values match those reported by McCarthy et al. (2008a, b)

$[V_0 = 402.03 (2) \text{ \AA}^3, K_0 = 136.5 (14) \text{ GPa}, \text{ and } K'_0 = 3.4 (4)]$  and Nestola et al. (2006)  $[V_0 = 402.26 (2) \text{ \AA}^3, K_0 = 134.0 (7) \text{ GPa}, \text{ and } K'_0 = 4.4 (1)]$ . The kosmochlor

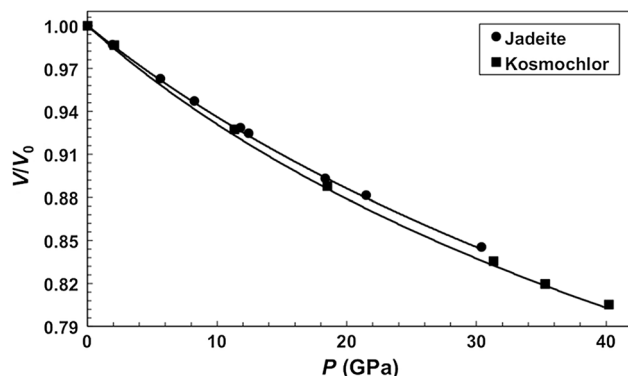


**Fig. 2** Normalized unit-cell volumes versus pressure for jadeite and kosmochlor. Kosmochlor, with a larger cell volume [ $V_0 = 420.0 (3) \text{ \AA}^3$ ] and smaller bulk modulus [ $K_0 = 123 (2) \text{ GPa}, K'_0 = 3.61 (9)$ ], is more compressible than jadeite [ $V_0 = 402.5 (4), K_0 = 136 (3), \text{ GPa}, K'_0 = 3.61 (9)$ ], which is consistent with previous studies (Thompson and Downs 2004; McCarthy et al. 2008a, b) that clinopyroxene compressibility is primarily controlled by the occupancy of M1

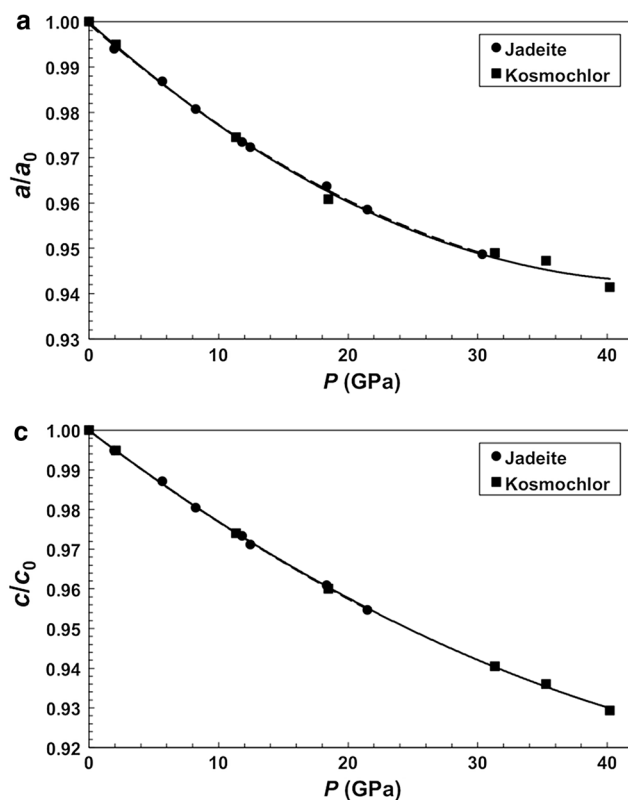
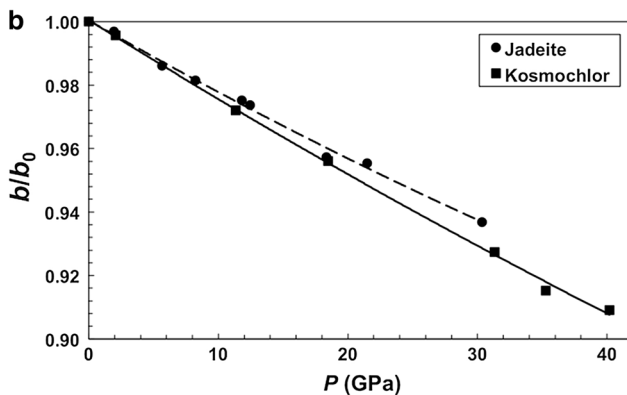


**Fig. 3** Normalized axial lengths versus pressure. Trendlines are dashed for jadeite and solid for kosmochlor. Jadeite and kosmochlor compressibilities are essentially identical along **a** and **c**, while kosmochlor compresses more rapidly along **b**. This is consistent with previ-

$K_0$  value that we obtained is a little lower than the values reported by Origlieri et al. (2003) [ $V_0 = 418.84 (3) \text{ \AA}^3, K_0 = 134.0 (7) \text{ GPa}, \text{ and } K'_0 = 3.7 (6)$ ] and Boffa Ballaran et al. (2009) [ $V_0 = 418.76 (2) \text{ \AA}^3, K_0 = 130.2 (7) \text{ GPa}, \text{ and } K'_0 = 4.1 (2)$ ].  $P$ - $V$  data and fitted curves are plotted in Fig. 1. The compressibility of jadeite and kosmochlor, expressed as  $V/V_0$ , is shown in Fig. 2. Unit-cell parameters for both minerals decrease with significant nonlinearity, with the exception of **b**, which, while decreasing the most rapidly of the three axes, exhibits the most linear trend (Fig. 3a–c). Unit-cell parameters **a** and **c** decrease at nearly identical rates for jadeite and kosmochlor, while **b** is more sensitive to composition with the rate of shortening,  $d(x/x_0)/dP$ , in kosmochlor decreasing approximately 1.1 times greater than in jadeite.

Unit-strain ellipsoids were constructed using cell parameters and STRAIN software (Ohashi 1982) to assess the degree of anisotropy between principal stress directions. In the pressure range of 0–30.4 (1) GPa, the unit-strain axial ratios for jadeite are 1.00:1.95:2.09. In the pressure range of 0–40.2 (1) GPa, the unit-strain axial ratios for kosmochlor are 1.00:2.15:2.43. The middle values represent strain symmetrically constrained to lie parallel to **b**. Strain



ous suggestions that the compressibility of the entire unit cell and **b** axis is primarily controlled by the compressive strength of the  $M1O_6$  chains (Thompson and Downs 2004; McCarthy et al. 2008a, b)

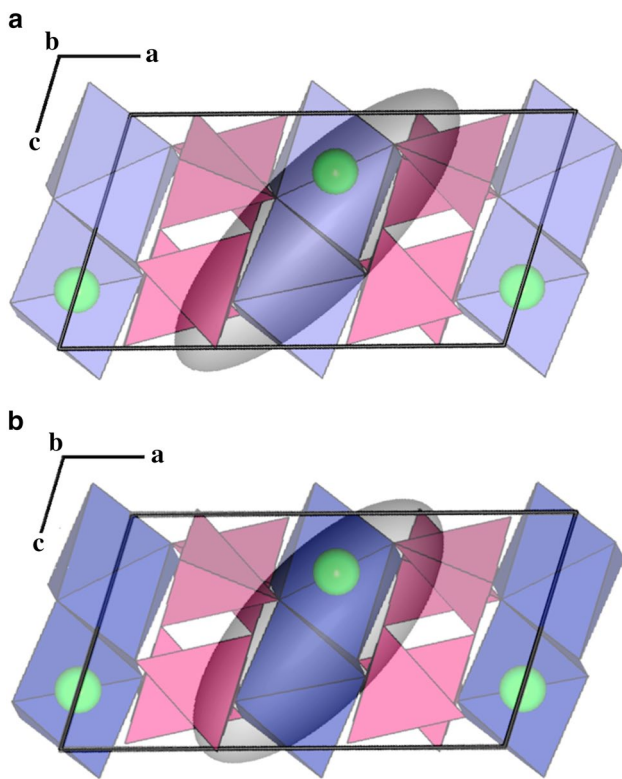


**Fig. 4** Oriented unit-strain ellipsoid superimposed on the **a** kosmochlor and **b** jadeite structures at ambient pressure viewed down **b**. M2 (Na) is illustrated as a sphere

**Table 5** Unit-strain ellipsoid parameters for jadeite and kosmochlor

Sample	$\Delta P$ (GPa)	Axes ( $\text{GPa}^{-1}$ ) ( $\times 10^2$ )			Orientation $\angle(\epsilon_3^a c)$ ( $^\circ$ )
		$\epsilon_1$	$\epsilon_2/b$	$\epsilon_3$	
Jadeite	30.4 (1)	0.107 (9)	0.208 (16)	0.222 (7)	30.5 (3)
Kosmo- chlor	40.2 (1)	0.093 (7)	0.200 (5)	0.226 (11)	28.3 (2)

ellipsoids are shown with respect to the ambient pressure crystal structure for both phases in Fig. 4. The axial values of the unit-strain ellipsoid and orientation of maximum strain directions are listed in Table 5. We compare our strain data with previous studies of jadeite to 8.31 GPa (Nestola et al. 2006) and 9.17 GPa (McCarthy et al. 2008a, b) and of kosmochlor to 6.80 GPa (Boffa Ballaran et al. 2009) and 9.28 GPa (Origlieri et al. 2003). Our results indicate that strain anisotropy in kosmochlor remains tri-axial (i.e.  $\epsilon_3 > \epsilon_2 > \epsilon_1$ ) throughout the pressure range of study but undergoes an abrupt reduction from 1.00:1.88:2.15 at 11.3 (1) GPa to 1.00:1.74:1.89 at 18.5 (1) GPa, which may be associated with an M2-coordination change, as described in the next section. Strain in jadeite approaches oblate uniaxial ( $\epsilon_3 \approx \epsilon_2 > \epsilon_1$ ) with a projected intersection of  $\epsilon_2$  and

$\epsilon_3$  at  $\sim 40$  GPa. Figure 5 illustrates the degree of anisotropy of the middle and maximum shortening directions,  $\epsilon_2$  and  $\epsilon_3$ , respectively, normalized to  $\epsilon_1$ , as a function of pressure.

Procrystal electron density distribution analysis indicates six Na–O bonds in both minerals at ambient conditions (Origlieri et al. 2003; McCarthy et al. 2008a, b). Sodium resides on a twofold symmetry axis, which constrains its coordination to an even number. At ambient conditions, Na is bonded to two O1, two O2, and two bridging O3 and symmetrically equivalent atoms, O3<sub>2</sub> and O3<sub>3</sub>, following the nomenclature of Downs (2003). Compression data from previous studies (Origlieri et al. 2003; McCarthy et al. 2008a, b) were used to predict a  $C2/c \rightarrow C2/c$  bonding transition at pressures of approximately 20 GPa when extrapolated Na–O3<sub>1,4</sub> and Na–O3<sub>2,3</sub> bonds shortened to the same length. Procrystal electron density analysis based on the data from the current study shows that Na in jadeite remains six-coordinated at 21.5 (1) GPa, while kosmochlor assumes eightfold coordination in between 9.28 (Origlieri et al. 2003) and 18.5 (1) GPa (Fig. 6). The longest Na–O “bonds” in kosmochlor at ambient conditions (Na–O3<sub>1,4</sub>) appear to decrease with slight nonlinearity. At pressures greater than 31.3 (1) GPa, the longest Na–O bonds are, in fact, Na–O3<sub>2,3</sub>. This crossover has also been observed in M2 (Ca–O) bonds in hedenbergite at  $\sim 4.5$  GPa (Zhang et al. 1997). Although the large spacing of our pressure steps limits the resolution of this coordination change and compression trend in kosmochlor, an abrupt decrease in strain anisotropy between 11.3(1) and 18.5(1) GPa, as shown in Fig. 5a, suggests the transition occurs within this pressure region. Extrapolation of Na–O3 bond lengths in jadeite suggests that Na will assume eightfold coordination by at least 27.5 GPa, at which point  $r(\text{Na–O3}_{1,4}) = r(\text{Na–O3}_{2,3})$ . This is most likely an overestimate; however, as procrystal electron density analysis reveals that the coordination change in kosmochlor occurs while Na–O3<sub>1,4</sub> bonds are still longer than Na–O3<sub>2,3</sub>.

The Al atom in jadeite and Cr atom in kosmochlor resides in an octahedral M1-site that remains six-coordinated with oxygen in both minerals throughout the pressure range of this study. A twofold symmetry axis runs through the M1 atoms maintaining three sets of two equivalent oxygen atoms. Polyhedral distortion is indexed using quadratic elongation, and bond angle variance measurements such that regular polyhedra have quadratic elongation values of 1, bond angle variance values of zero, and distorted polyhedra have quadratic elongation values greater than 1 and positive bond angle variance (Robinson et al. 1971). The distortion of the Al octahedra in jadeite remains relatively constant with pressure and shows little variation in the aforementioned distortion indices (Fig. 7). The Cr octahedron, however, becomes increasingly irregular with pressure above 18.5 (1) GPa. The mean octahedral angle

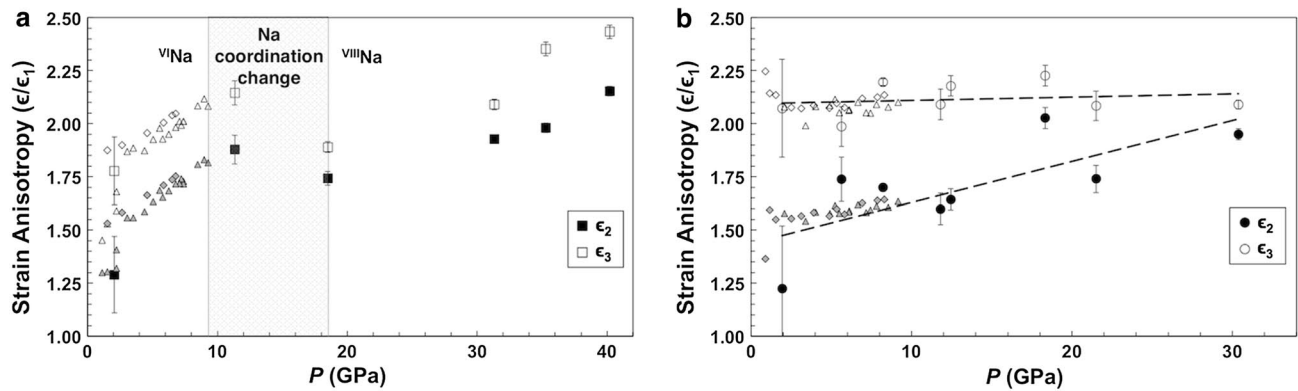


**Fig. 5** Degree of anisotropic strain as a function of pressure in **a** kosmochlor and **b** jadeite. The kosmochlor strain ellipsoid is tri-axial to 40.2 (1) GPa with an abrupt decrease in anisotropy between approximately 11–18 GPa, which corresponds with the pressure interval that Na changes from six to eight coordination, as verified through pro-crystal electron density distribution analysis. The maximum strain direction,  $\epsilon_3$ , in jadeite does not undergo additional compression

throughout the pressure range of study, relative to  $\epsilon_1$ , while the intermediate ( $\epsilon_2$ ) continues to decrease. The jadeite strain ellipsoid is predicted to become oblate uniaxial ( $\epsilon_2 = \epsilon_3$ ) at ~40 GPa. Large filled ( $\epsilon_2/\epsilon_1$ ) and unfilled ( $\epsilon_3/\epsilon_1$ ) data points are from this study, *small triangles* are from Origlieri et al. (2003) (kosmochlor) and McCarthy et al. (2008a, b) (jadeite), *small diamonds* are from Boffa Ballaran et al. (2009) (kosmochlor) and Nestola et al. (2006) (jadeite)

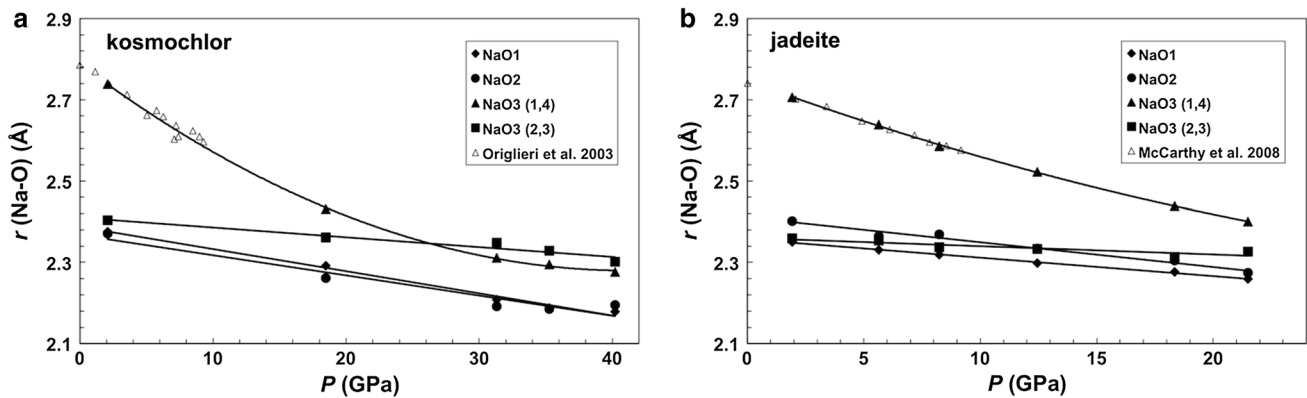


**Fig. 6** Variation of Na(M2)–O bond lengths in **a** kosmochlor and **b** jadeite with pressure at 298 K. Na coordination in kosmochlor changes from 6 to 8 in between 9.28 (Origlieri et al. 2003) and 18.5

(1) GPa. Na coordination in jadeite likely changes from six to eight between 24 and 28 GPa

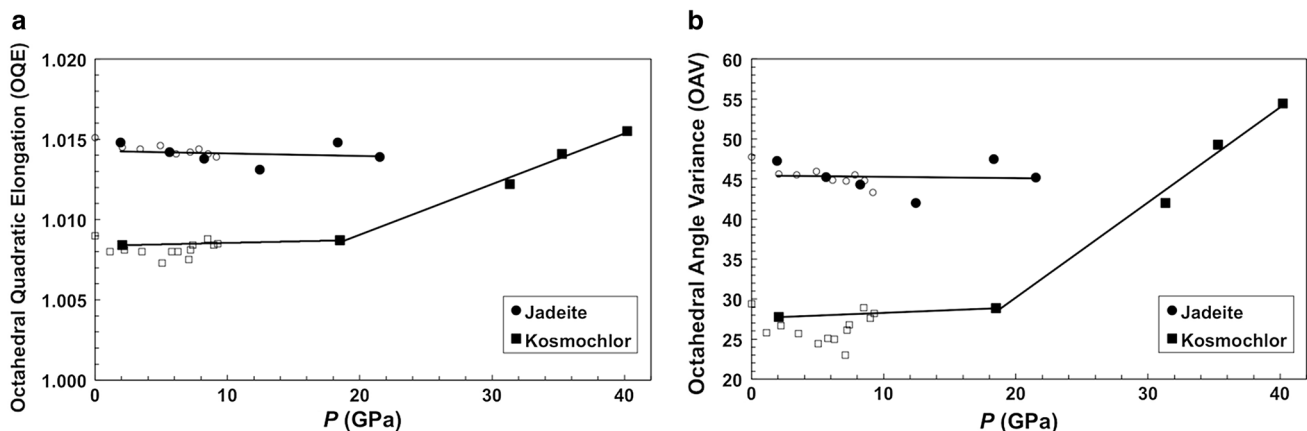


**Fig. 7** M1 polyhedral distortion indices in jadeite and kosmochlor as a function of pressure: **a** octahedral quadratic elongation, **b** octahedral angle variance. M1 in kosmochlor becomes increasingly dis-

torted above 18.5 (1) GPa, while M1 distortion in jadeite remains constant. *White-filled circle* and *square* data points are from McCarthy et al. (2008a, b) and Origlieri et al. (2003), respectively

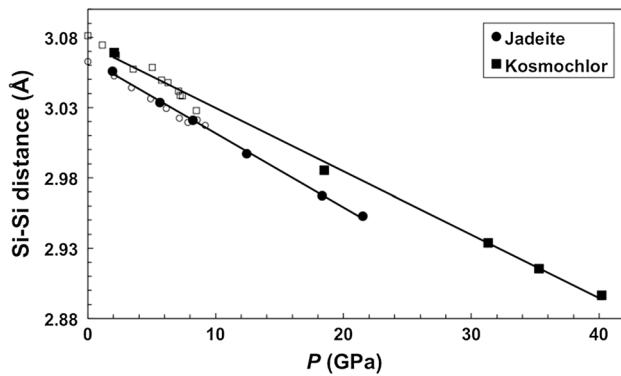


**Fig. 8** Si–Si distance in a Si–O–Si linkage in jadeite and kosmochlor as a function of pressure. White-filled circle and square data points are from McCarthy et al. (2008a, b) and Origlieri et al. (2003), respectively

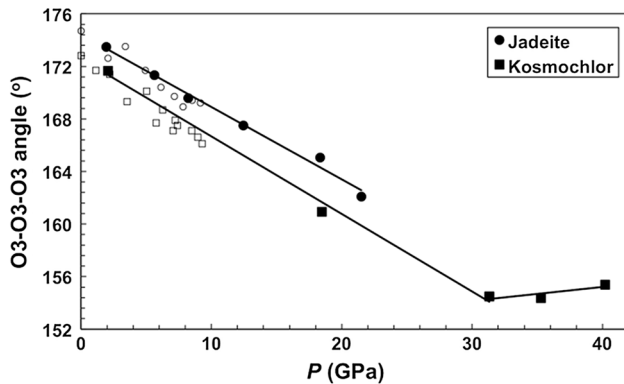


**Fig. 9** Tetrahedral chain kinking as measured by the O3–O3–O3 angle in jadeite and kosmochlor as a function of pressure. Tetrahedra reach a rotational limit at approximately 31 GPa while Si–Si distance (Fig. 8) decreases continuously. White-filled circle and square data points are from McCarthy et al. (2008a, b) and Origlieri et al. (2003), respectively

variance (OAV) in kosmochlor increases by a factor of 1.96, from 27.7456 at 2.1 (1) GPa to 54.4445 at 40.2 (1) GPa while the OAV in jadeite remains essentially unchanged at  $\sim 46.0$  (Fig. 7b). This difference is likely due to Cr's electronic configuration involving *d*-orbitals such that the  $\text{CrO}_6$  polyhedra are more easily deformed than  $\text{AlO}_6$  polyhedra, in addition to the observation that the M2-bonding transition at pressures lower than 18.5 (1) GPa may result in a more rapid deformation of the M1-octahedron.

The distance between Si atoms decreases linearly as a function of pressure in both minerals, as shown in Fig. 8. In jadeite, this strain is complimented by a linear decrease in the  $\angle\text{O3–O3–O3}$  of approximately  $-0.56^\circ/\text{GPa}$  (Fig. 9). Rotation of  $\text{SiO}_4$  tetrahedra in kosmochlor follows a similar trend ( $\sim -0.59^\circ/\text{GPa}$ ) to pressures of 31.3 (1) GPa at which point, increased chain kinking appears to become

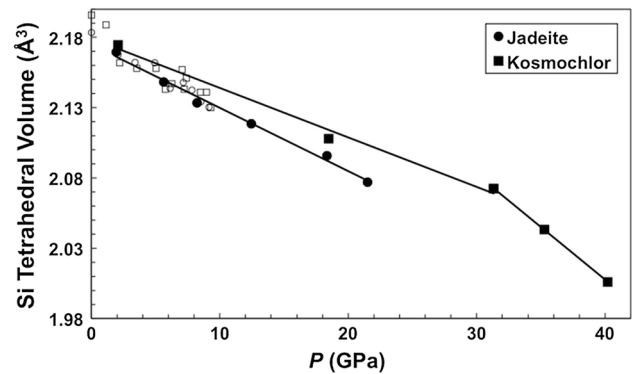


**Fig. 10**  $\text{SiO}_4$  tetrahedral volume in jadeite and kosmochlor as a function of pressure. Tetrahedral volume in kosmochlor decreases by approximately  $-3.5 (10^{-3}) \text{ \AA}^3/\text{GPa}$  below approximately 32 GPa and increases to approximately  $-7.5 (10^{-3}) \text{ \AA}^3/\text{GPa}$  above 32 GPa. Tetrahedral volume in jadeite decreases at a more consistent rate of approximately  $-4.4 (10^{-3}) \text{ \AA}^3/\text{GPa}$ . White-filled circle and square data points are from McCarthy et al. (2008a, b) and Origlieri et al. (2003), respectively

energetically unfavorable, and the O3–O3–O3 angle remains constant at  $\sim 154.8^\circ$  from 31.3 (1) to 40.2 (1) GPa (Fig. 9). These findings are consistent with the Webb and Jackson (1993) study on the pressure dependence on the elastic moduli of orthopyroxene,  $(\text{Mg}_{0.8}\text{Fe}_{0.2})\text{SiO}_3$ , in which they proposed that tetrahedral rotation would serve as the dominant compression mechanism in pyroxene only under a limited pressure range. Interestingly, the ceasing of tetrahedral chain kinking in kosmochlor is accompanied by a rapid increase in the rate of Si-tetrahedral compression from  $-3.5 (10^{-3}) \text{ \AA}^3/\text{GPa}$  up to 31.3 (1) GPa to  $-7.5 (10^{-3}) \text{ \AA}^3/\text{GPa}$  above 31.3 (1) GPa (Fig. 10). A similar discontinuity in both O3–O3–O3 angle and tetrahedral volume with increasing pressure was reported in orthoenstatite at lower pressure ( $\sim 4$  GPa) (Hugh-Jones and Angel 1994); however, this finding was refuted by Periotto et al. (2012) who re-investigated the crystal structure up to 9.4 GPa and did not measure the discontinuity, therefore attributing large refinement uncertainties to inaccurate conclusions regarding a change in compression mechanism. Nevertheless, the high-precision kosmochlor data of the present study exhibit a clear discontinuity in the rate of chain kinking and an increase by greater than a factor of two in the rate of Si-tetrahedral compression above 31 GPa. This “gridlock” of O3–O3–O3 angle and associated increase in tetrahedral compression may trigger a change in Si coordination from four to six at higher pressures, as observed in previous studies of high-pressure synthetic Na-clinopyroxenes which revealed Si to partially substitute into the octahedral M1-site (Angel et al. 1988; Konzett et al. 2005; Yang and Konzett 2005; Yang et al. 2009; Posner et al. 2012), or to transform to the  $\beta$ -phase with a conversion of

half of the corner-sharing  $\text{SiO}_4$  tetrahedral chains into layers of edge-sharing  $\text{SiO}_6$  octahedra as observed in natural diopside above 56.1 (1) GPa (Plonka et al. 2012).

## Summary

We report a series of high-pressure crystal structure refinements on natural jadeite and synthetic kosmochlor at ambient temperature. Our results are consistent with previous studies that propose clinopyroxene compression to be primarily controlled by the occupancy of the M1-site (Thompson and Downs 2004; McCarthy et al. 2008a, b). An M2-coordination change from 6 to 8 occurs between 9.28 (Origlieri et al. 2003) and 18.5 (1) GPa in kosmochlor, while Na remains in octahedral coordination in jadeite up to 21.5 (1) GPa. Kosmochlor undergoes a change in compression mechanism at ~31 GPa indicated by discontinuities in both the rate of the Si tetrahedral chain rotation and tetrahedral compression. Below 31 GPa, O3–O3–O3 angle and tetrahedral volume in kosmochlor decrease linearly with pressure, whereas above 31 GPa chain kinking ceases and the rate of Si tetrahedral compression with pressure increases by more than a factor of two. Such structural measurements were not observed in jadeite most likely because the M2-coordination change did not occur within the pressure range of the present study. Additional high-pressure crystal structure refinements on jadeite at higher pressure, or other Na-pyroxenes such as aegirine, namansilitite, or natallyite with  $\text{Fe}^{3+}$ ,  $\text{Mn}^{3+}$ , and  $\text{V}^{3+}$  in M1, respectively, may reveal similar compression behavior and could be used to model pyroxene stability at transition zone pressures.

**Acknowledgments** We thank Dr. Fabrizio Nestola for his helpful review and the editor for handling our manuscript. E. S. P. wishes to acknowledge the Downs Research Group for supporting her participation in this project. P. D. wishes to acknowledge National Science Foundation Division of Earth Sciences Geophysics Grant No. 1344942. Portions of this work were performed at GeoSoilEnviroCARS (Sector 13), Advanced Photon Source (APS), Argonne National Laboratory. GeoSoilEnviroCARS is supported by the National Science Foundation—Earth Sciences (EAR-1128799) and Department of Energy—Geosciences (DE-FG02-94ER14466). Use of the Advanced Photon Source was supported by the U. S. Department of Energy, Office of Science, Office of Basic Energy Sciences, under Contract No. DE-AC02-06CH11357.

## References

- Akaogi M, Tanaka A, Kobayashi M, Fukushima N, Suzuki T (2002) High-pressure transformations in  $\text{NaAlSi}_3\text{O}_8$  and thermodynamic properties of jadeite, nepheline, and calcium ferrite-type phase. *Phys Earth Planet Inter* 130:49–58
- Angel RJ, Gasparik T, Ross NL, Finger LW, Prewitt CT, Hazen RM (1988) A silica-rich sodium pyroxene with six-coordinations silicic. *Nature* 335:156–158
- Bell PM, Roseboom EH (1969) Melting relations of jadeite and albite to 45 kilobars with comments on melting diagrams of binary systems at high pressures. *Mineral Soc Am Spec Pap* 2:151–161
- Birch F, LeCompte P (1960) Temperature pressure plane for albite composition. *Am J Sci* 258:209–217
- Boffa Ballaran T, Nestola F, Tribaudino M, Ohashi H (2009) Bulk modulus variation along the diopside–kosmochlor solid solution. *Eur J Mineral* 21:591–597
- Cameron M, Sueno S, Prewitt CT, Papike JJ (1973) High-temperatures crystal chemistry of acmite, diopside, hedenbergite, jadeite, spodumene, and ureyite. *Am Mineral* 58:594–618
- Clark JR, Appleman DE, Papike JJ (1969) Crystal-chemical characterization of clinopyroxenes based on eight new structure refinements. *Mineral Soc Am Spec Pap* 2:31–50
- Dera P, Lazarz JD, Lavina B (2011) Pressure-induced development of bonding in NiAs type compounds and polymorphism of NiP. *J Solid State Chem* 184:1997–2003
- Dera P, Zhuravlev K, Prakapenka V, Rivers ML, Finkelstein GJ, Grubor-Urosevic O, Tschauer O, Clark SM, Downs RT (2013) High-pressure single-crystal micro-X-ray diffraction ( $\text{SC}\mu\text{XRD}$ ) analysis with GSE\_ADA/RSV software. *High Press Res* 33:466–484
- Downs RT (2003) Topology of the pyroxenes as a function of temperature, pressure and composition determined from the procrystal electron density. *Am Mineral* 88:556–566
- Harlow GE (1997) K in clinopyroxene at high pressure and temperature: an experimental study. *Am Mineral* 82:259–269
- Harlow GE, Olds EP (1987) Observations on terrestrial ureyite and ureyitic pyroxene. *Am Mineral* 72:126–136
- Holland TJB (1980) Reaction albite = jadeite + quartz determined experimentally in the range 600–1200°C. *Am Mineral* 65:129–134
- Hugh-Jones DA, Angel RJ (1994) A compressional study of  $\text{MgSiO}_3$  orthoenstatite up to 8.5 GPa. *Am Mineral* 79:405–410
- Hugh-Jones D, Sharp T, Angel R, Woodland A (1996) The transition of orthoferrosilite to high-pressure  $C2/c$  clinoferrosilite at ambient temperature. *Eur J Mineral* 8:1337–1345
- Kawai K, Tsuchiya T (2012) High-P, T phase relations in the  $\text{NaAl-Si}_2\text{O}_6$  system from first principles computation. *Phys Chem Miner* 39:305–310
- Konzett J, Yang H, Frost DJ (2005) Phase relations and stability of magnetoplumbite- and crichtonite-series phases under upper-mantle P–T conditions: an experimental study to 15 GPa with implications for LILE metasomatism in the lithospheric mantle. *J Petrol* 46:749–781
- Liu L (1978) High-pressure phase transformation of albite, jadeite, and nepheline. *Earth Planet Sci Lett* 4:183–186
- Mao HK, Xu J, Bell PM (1986) Calibration of the ruby pressure gauge to 800 kbar under quasi-hydrostatic conditions. *J Geophys Res* 91:4673–4676. doi:10.1029/JB091iB05p04673
- McCarthy AC, Downs RT, Thompson RM (2008a) Compressibility trends of the clinopyroxenes, and in situ high-pressure single-crystal X-ray diffraction study of jadeite. *Am Mineral* 93:198–209
- McCarthy AC, Downs RT, Thompson RM, Redhammer GJ (2008b) In situ high-pressure single-crystal X-ray study of aegirine,  $\text{NaFe}^{3+}\text{Si}_2\text{O}_6$ , and the role of M1 size in clinopyroxene compressibility. *Am Mineral* 93:1829–1837
- Nestola F, Boffa Ballaran T, Liebske C, Bruno M, Tribaudino M (2006) High-pressure behavior along the jadeite  $\text{NaAl}_2\text{O}_6$ -aegirine  $\text{NaFeSi}_2\text{O}_6$  solid solution up to 10 GPa. *Phys Chem Miner* 33:222–227

- Nestola F, Boffa Ballaran T, Liebske C, Thompson R, Downs RT (2008) The effect of the hedenbergite substitution on the compressibility of jadeite. *Am Mineral* 93:1005–1013
- Newton RC, Smith JV (1967) Investigations concerning the breakdown of albite at depth in the earth. *J Geol* 75:268–286
- Nimis P (2002) The pressures and temperatures of formation of diamond based on thermobarometry of chromian diopside inclusions. *Can Mineral* 40:871–884
- Nimis P, Taylor WR (2000) Single pyroxene thermobarometry for garnet peridotites. I. Calibration and testing of a Cr-in-Cpx barometer and an enstatite-in-Cpx thermometer. *Contrib Miner Petrol* 139:541–554
- Ohashi Y (1982) A program to calculate the strain tensor from two sets of unit-cell parameters (STRAIN). In: Hazen RM, Finger LW (eds) *Comparative crystal chemistry*. Wiley, New York, pp 92–102
- Origlieri MJ, Downs RT, Thompson RM, Pommier CJS, Denton MB, Harlow GE (2003) High-pressure crystal structure of kosmochlor,  $\text{NaCrSi}_2\text{O}_6$ , and systematics of anisotropic compression in pyroxenes. *Am Mineral* 88:1025–1032
- Periotto B, Balic-Zunic T, Nestola F, Katerinopoulou A, Angel RJ (2012) Re-investigation of the crystal structure of enstatite under high-pressure conditions. *Am Mineral* 97:1741–1748
- Plonka AM, Dera P, Irmen P, Rivers ML, Ehm L, Parise JB (2012)  $\beta$ -diopside, a new ultrahigh-pressure polymorph of  $\text{CaMgSi}_2\text{O}_6$  with six-coordinated silicon. *Geophys Res Lett* 39:L24307. doi: [10.1029/2012GL054023](https://doi.org/10.1029/2012GL054023)
- Posner ES, Konzett J, Frost DJ, Downs RT, Yang H (2012) High-pressure synthetic  $(\text{Na}_{0.97}\text{Mg}_{0.03})(\text{Mg}_{0.43}\text{Fe}_{0.17}^{3+}\text{Si}_{0.40})\text{Si}_2\text{O}_6$ , with six-coordinated silicon, isostructural with *P2/n* omphacite. *Acta Crystallogr A* E68(2):i18
- Prewitt CT, Burnham CW (1966) The crystal structure of jadeite,  $\text{NaAlSi}_2\text{O}_6$ . *Am Mineral* 51:956–975
- Rivers M, Prakapenka VB, Kubo A, Pullins C, Holl CM, Jacobsen SD (2008) The COMPRES/GSECARS gas-loading system for diamond anvil cells at the Advanced Photon Source. *High Press Res* 28:273–292
- Robinson K, Gibbs GV, Ribbe PH (1971) Quadratic elongation: a quantitative measure of distortion in coordination polyhedra. *Science* 172:567–570
- Secco L, Martignago F, Dal Negro A, Reznitskii LZ, Sklyarov EV (2002) Crystal chemistry of  $\text{Cr}^{3+}$ - $\text{V}^{3+}$ -rich clinopyroxenes. *Am Mineral* 87:709–714
- Sheldrick GM (2008) A short history of SHELX. *Acta Crystallogr A* A64:112–122
- Taylor SR, McLennan SM (1985) *The continental crust: its composition and evolution*. Blackwell, Carlton
- Thompson RM, Downs RT (2003) Model pyroxenes I: ideal pyroxene topologies. *Am Mineral* 88:653–666
- Thompson RM, Downs RT (2004) Model pyroxenes II: structural variation as a function of tetrahedral rotation. *Am Mineral* 89:614–628
- Webb SL, Jackson I (1993) The pressure dependence of the elastic moduli of single-crystal orthopyroxene  $(\text{Mg}_{0.8}\text{Fe}_{0.2})\text{SiO}_3$ . *Eur J Mineral* 5:1111–1119
- Woodland AB (1998) The orthorhombic to high-P monoclinic phase transition in Mg-Fe pyroxenes: can it produce a seismic discontinuity? *Geophys Res Lett* 25:1241–1244
- Yagi A, Suzuki T, Akaogi M (1994) High pressure transitions in the system  $\text{KAlSi}_3\text{O}_8$ - $\text{NaAlSi}_3\text{O}_8$ . *Phys Chem Miner* 21:12–17
- Yang H, Konzett J (2005) Crystal chemistry of a high-pressure *C2/c* clinopyroxene with six-coordinated silicon. *Am Mineral* 90:1223–1226
- Yang H, Prewitt CT (2000) Chain and layer silicates at high temperatures and pressures. In: Hazen RM, Downs RT (eds) *High-temperature and high-pressure crystal chemistry*, 41. Reviews in mineralogy and geochemistry. Mineralogical Society of America, Chantilly, pp 211–255
- Yang H, Konzett J, Frost DJ, Downs RT (2009) X-ray diffraction and Raman spectroscopic study of clinopyroxenes with six-coordinated Si in the  $\text{Na}(\text{Mg}_{0.5}\text{Si}_{0.5})\text{Si}_2\text{O}_6$ - $\text{NaAlSi}_2\text{O}_6$  system. *Am Mineral* 94:942–949
- Zhang L, Ahsbahs H, Hafner SS, Kutoglu A (1997) Single-crystal compression and crystal structure of clinopyroxene up to 10 GPa. *Am Mineral* 82:245–258